USCAP

Check for updates

ARTICLE

Recurrent *YAP1::MAML2* fusions in "nodular necrotizing" variants of myxoinflammatory fibroblastic sarcoma: a comprehensive study of 7 cases

Raul Perret [1 ✉], Matthias Tallegas[2], Valérie Velasco[1], Isabelle Soubeyran[1], Jean-Michel Coindre[1,3], Rihab Azmani[4], Jessica Baud[3,5], Guillaume Bacle[6], Gonzague De Pinieux[2] and François Le Loarer [1,3,5]

Myxoinflammatory fibroblastic sarcoma (MIFS) is a rare soft tissue tumor with a predilection for the distal extremities and a tendency for local recurrence. Morphologically, MIFS consists of spindle and bizarre epithelioid cells resembling virocytes embedded in a fibrous to myxoid stroma with an abundant inflammatory infiltrate. Importantly, the molecular landscape of MIFS is wide and includes: *VGLL3* amplification, *BRAF* fusion/amplification and *OGA/TGFBR3* rearrangements. In this study, we describe a variant of MIFS showing a frequent nodular configuration associated with necrosis and recurrent *YAP1::MAML2* fusions. The cohort consisted of 7 patients (4 females and 3 males) ranging in age from 21 to 71 years (median: 47 years). Two tumors (28%) occurred in acral locations while the remaining cases were more widely distributed (thigh, $n = 2$; arm, $n = 1$; neck; $n = 1$; chest-wall, $n = 1$). Tumor size ranged from 10 to 38 mm (median: 20 mm). Histologically, lesions frequently presented as nodules with central areas of necrosis, and were predominantly composed of sheets of epithelioid cells with large vesicular nuclei and prominent nucleoli (Reed-Sternberg-like cells or virocytes). The stroma was mostly fibrous and showed a polymorphous inflammatory infiltrate. Myxoid stromal changes were focally seen in one case, and pseudolipoblasts were absent. The immunophenotype was nonspecific, with only pan-keratin (AE1-AE3) and cyclin D1 expression in a subset of cases. RNA-Sequencing detected *YAP1::MAML2* fusions in 3/7 cases; aCGH showed no significant gene copy number variations in 4 tested cases, and FISH analysis showed no *VGLL3* amplification in 1 tested case. Follow-up was available for 6 cases, ranging from 7 to 63 months (median: 42 months). Local recurrence and metastasis were not seen and one tumor showed spontaneous regression following initial biopsy. In conclusion, we describe a novel variant of MIFS with distinctive clinicopathological and molecular features for which we propose the term "nodular necrotizing" MIFS.

INTRODUCTION

Myxoinflammatory fibroblastic sarcoma (MIFS) is a rare and diagnostically challenging mesenchymal tumor with a tendency for local recurrence (~50% of cases) and rare distant spread[1]. Most examples occur in the distal limbs of adults with a roughly equal gender distribution. Histologically, MIFS generally presents as an infiltrative mass composed of spindle and epithelioid cells embedded in an alternating fibrous to myxoid stroma with a prominent inflammatory infiltrate[2]. Importantly, the epithelioid cells have a distinctive appearance with large vesicular nuclei and prominent nucleoli, closely resembling Reed-Sternberg cells or "virocytes." In classic cases, mitotic activity is low (<1/mm²) and necrosis is rare and focal (~14% of cases), but cases with increased mitotic activity (including atypical forms) and/or hypercellular areas have been reported in the literature[1].

Immunohistochemistry has a limited role in the diagnosis of MIFS as most cases have a nonspecific profile showing variable expression of CD34 (~50% of cases), keratins (~30% of cases),

CD68, alpha-smooth muscle actin, desmin, Cyclin D1 and Factor XIIIa[1,3]. Molecular techniques are infrequently used in the diagnostic workup of MIFS, but their recent application for research has shed some light on the pathogenesis of these cryptic tumors. The molecular landscape of MIFS is heterogeneous with three recurrent molecular aberrations known to date: 1-*VGLL3* amplification[4]; 2-*OGA* (*MGEA5*) and/or *TGFBR3* rearrangements[4]; and rarely 3- *BRAF*-related alterations[5]. The exact incidence of these aberrations is currently unknown, but it appears that *VGLL3* amplification is the most consistent anomaly, seen in roughly 40% of cases[3].

Over the past years, we have come to identify an unusual variant of MIFS frequently manifesting as a single nodule with central necrosis and characterized by a predominance of plump virocyte-like cells, lack of myxoid stroma and recurrent *YAP1::MAML2* fusions. The purpose of this study was to describe the clinicopathological, immunohistochemical and molecular features of this distinctive variant of MIFS.

[1]Department of Biopathology, Institut Bergonié, Comprehensive Cancer Center, F-33000 Bordeaux, France. [2]Department of Pathology, Hôpital Trousseau–CHU de Tours, Avenue de la République, 37170 Chambray-lès-Tours, France. [3]University of Bordeaux, Talence, France. [4]Department of Bioinformatics, Institut Bergonie, Bordeaux, France. [5]INSERM U1218, ACTION Unit, Bordeaux, France. [6]Department of Orthopaedic Surgery, Hand Surgery Unit, Hôpital Trousseau–CHU de Tours, Avenue de la République, 37170 Chambray-lès-Tours, France. ✉email: r.perret@bordeaux.unicancer.fr

MATERIALS AND METHODS
Study design
The archives of Bergonié Institute were searched for cases coded as "nodular necrotizing myxoinflammatory fibroblastic sarcoma" (NN-MIFS) and "unclassified atypical inflammatory lesion" (a descriptive term initially used by the authors), yielding 6 cases. An additional case (case 5) was identified following the detection of a YAP1::MAML2 fusion in a biopsy of a MIFS, which had been sent to our center for molecular studies. All available material was reviewed, including hematoxylin, eosin and saffron (HES) stains, immunohistochemistry, and molecular assays performed during the initial diagnostic workup. Additional immunohistochemical markers were conducted in all cases, and total RNA sequencing was performed retrospectively in cases 1–4. Clinical information and follow-up data were recovered from the referring pathologists and direct communication with the treating physicians.

All cases are recorded in the French expert sarcoma network (RRePS) database, which is approved by the National Committee for Protection of Personal Data (CNIL, no. 910390).

Immunostaining
Immunohistochemistry was carried out on 4 micrometers paraffin sections as per standard technique on a Ventana Benchmark ULTRA automat (Ventana, Roche Tissue Diagnostics, Oro Valley, Arizona, USA). The following antibodies were used: Pan-Keratin (AE1/AE3/PCK26; Prediluted; Roche Tissue Diagnostics); Desmin (DE-R-11; Prediluted; Roche Tissue Diagnostics); S100 (Rabbit polyclonal; 1:2000; Agilent Dako, Santa Clara, California, USA); CD34 (QBEnd10; Prediluted; Roche Diagnostics) and YAP1-CT (D8H1x; 1:100; Cell Signaling, Danvers, Massachusetts, USA); Cyclin D1 (rabbit monoclonal, SP4-R; Prediluted; Roche Diagnostics). In cases 2, 3 and 4, additional markers and special stains performed in the referring institutions were pulled-out from our archives and reviewed (see results section). Expression was considered diffusely positive if staining was present in >75% of tumor cells, focally positive if staining was present in 1-75% of tumor cells, and negative if no staining was seen.

Array-comparative genomic hybridization
Array-Comparative genomic hybridization (aCGH) was performed in cases 1, 2, 4 and 7. Briefly, genomic DNA was extracted from FFPE material using a commercially available kit (QIAamp® DNA FFPE Tissue Kit; QIAGEN, Hilden, Germany). DNA was hybridized onto 8 × 60 K whole-genome arrays (G4450A; Agilent Technologies, Santa Clara, California, USA) according to the manufacturer's protocol. Microarray slides were scanned using a DNA Microarray Scanner, and images were analyzed using Feature Extraction V10.1.1.1. Data were analyzed using the Agilent Cytogenomics software 4.0.3.12 (Agilent).

Fluorescence in-situ hybridization
Fluorescence in situ hybridization (FISH) analysis was performed on interphase nuclei from 4-µm-thick sections of FFPE tissue using the following custom probes made by bacterial artificial chromosomes (BAC): RP11-473N10 and RP11-36C2 covering the VGLL3 gene and three control probes RP11-933C22, RP11-787C24 and RP11-280N18 located in chromosome 3 (Empire Genomics, Buffalo, New York, USA). DNA from each BAC was isolated as per the manufacturer's instructions. The BAC clones were labeled with fluorochromes by nick translation and validated on normal metaphase chromosomes. For the interpretation, at least 100 non-overlapping intact nuclei were counted, and the presence of VGLL3 amplification was assessed using the criteria proposed by Antonescu et al.[6]

Total RNA-Sequencing
Total RNAs were extracted from FFPE material using the Maxwell RSC FFPE plus DNA Kit (Promega Corporation, Madison, Wisconsin, USA), as per the manufacturer's recommendations. The quantity of total RNA was assessed using Qubit (Thermo Fisher Scientific). The quality of total RNA was evaluated with the Agilent RNA 6000 Nano kit (Agilent Technologies) and the 2100 Bioanalyzer Instrument (Agilent Technologies) using a cutoff of DV200 above 20%. Library constructions were performed using the Truseq RNA exome Kit (Illumina, San Diego, USA). Paired-end RNA-sequencing was performed with the NextSeq 500/550 High Output V2 kit (150 cycles) on the Illumina NextSeq 500 Sequencing System (Illumina, San Diego, USA). All reads were independently aligned with FusionMap (version 10.0.1.29.) against the hg19 version of the human reference genome. Sequencing reads were analyzed with Defuse, Starfusion, FusionMap and FusionInspector tools for fusion transcript detection.

Gene expression profiling
The gene expression profiles of NN-MIFS (n = 6) were compared with a control group, including classic examples of MIFS (n = 8) and superficial CD34-positive fibroblastic tumor/PRDM10-rearranged soft tissue tumor (SCD34FT/PRDM10-STT, n = 15). Clinicopathological and molecular information of the control cohort can be accessed online (Supplementary Table 1). Of note, one case of a NN-MIFS (case 1) did not pass quality control and was excluded from the analysis (<5,000,000 total raw read counts compared to ≥5,000,000 in all other samples).

Counts of sequences at the gene level were calculated using HtSeq version 0.6.0[7]. For RNA-Sequencing analysis of quantitative expression values, gene count data were normalized according to the VOOM method[8], which transforms raw count values to log2-counts per million (logCPM), estimates the mean-variance relationship and uses this relationship to compute appropriate observational-level weights. Clustering was performed with the R package Cluster ConsensusClusterPlus[9] using 1000 permutations on the subset of samples obtained by leave-n-out of 40% of samples. Unsupervised clustering analysis of RNA-Sequencing expression data was performed using agglomerative hierarchical clustering with distance criteria (1-Pearson_Correlation) and linkage criteria equal to average via the function hclust available in R[10].

RESULTS
Clinical findings
The study cohort consisted of 4 females and 3 males with a median age at presentation of 47 years (Table 1). The lesions predominantly occurred in the extremities (5/7 tumors, 71%), including the thigh (n = 2), the arm (n = 1), the hand (n = 1) and the finger (n = 1). The other primary sites were the neck and the chest wall (one case each). Three tumors (43%) were described as painful and showed signs of local inflammation leading to treatment with antibiotics in two cases. All lesions were solitary at presentation, and two tumors (cases 1 and 5) were reported to evolve for "weeks" before consultation.

Clinical follow-up information was available for 6 cases (86%), with a median follow-up duration of 42 months (range: 7–63 months). Most lesions were excised (6/7), and the majority showed at least focally positive margins (5/6), leading to a complementary re-excision in 2 cases. All patients with available follow-up were alive without evidence of disease at the latest control. The only tumor that was not excised (case 5) occurred in a 71-year-old male who presented with a 38 mm inflammatory hand mass showing a necrotic center on MRI (Fig. 1A). On biopsy, the pathology findings led to the hypothesis of an inflammatory pseudotumor and possibly an atypical mycobacterial infection, which yielded empiric antibiotic therapy and additional sampling (for microbial culture and histopathological analysis). Microbial culture did not reveal any pathogen, and a diagnosis of MIFS was subsequently proposed upon a second expert opinion and the review of all available material. Surgical excision (transmetacarpal amputation) was proposed, but the patient refused due to decreased pain and inflammation. Clinical and radiological surveillance showed a marked decrease in symptoms and tumor size at 14 months following the initial consultation, followed by complete regression. The patient was alive without evidence of disease at the latest control (45 months after initial diagnosis).

Pathological and immunohistochemical findings
The histopathological and main immunohistochemical findings are summarized in Table 1 and Figs. 1, 2. Tumor size was available in 5 cases and varied from 10 to 38 mm (median and mean: 20 mm). The following diagnoses and differentials were mentioned by the referring pathologists: inflammatory pseudotumor (n = 2); inflammatory myofibroblastic tumor (n = 1); reticulohistiocytoma (n = 1); myxoinflammatory fibroblastic sarcoma (n = 1); angiomatoid fibrous histiocytoma (n = 1); epithelioid sarcoma (n = 1); pleomorphic sarcoma (n = 1).

Histologically, at low power, most excised tumors (4/6) consisted of relatively well-circumscribed nodules centered on

Table 1. Clinicopathological and immunohistochemical features of "nodular necrotizing" myxoinflammatory fibroblastic sarcoma.

Case	Age/Sex	Tumor size (mm)	Location	Mitotic activity 10 HPF/ mm²	CD34	Keratin	Cyclin D1	Treatment	Vital Status/Follow-up (months)
1	21/F	20	thigh	1/0.4ᵃ	—	—	+	Antibiotic therapy then incomplete excision	AWED/63
2	58/F	na	thigh	3/1.2	—	+/−	+	Complete excision	AWED/62
3	47/F	20	arm	9/3.8	—	+/−	+	Incomplete excision	AWED/40
4	31/F	15	chest wall	2/0.8	—	—	+	Incomplete excision then reexcision	AWED/29
5	71/M	38	hand	2/0.8	—	—	np	Antibiotic therapy	AWED/45
6	44/M	na	neck	3/1.2	—	+/−	np	Incomplete excision then reexcision	AWED/7
7	62/M	10	finger	1/0.4	—	+/−	np	Incomplete excision	na

np not performed, *na* not available, *AWED* alive without evidence of disease.
ᵃAtypical mitotic figure.

the deep dermis or hypodermis (Fig. 2A and Supplementary Fig. 1). Of note, the silhouette of two tumors could not be assessed adequately due to the quality of the excision (intralesional). All tumors were associated with a moderate to dense inflammatory infiltrate, generally comprising peripheral areas rich in lympho-cytes and plasma cells, and central regions rich in neutrophils and eosinophils. The tumors were predominantly composed of sheets of bizarre epithelioid cells with variably abundant eosinophilic and glassy cytoplasm, and one or multiple large and irregular vesicular nuclei with prominent macronucleoli ("virocytes" or Reed-Sternberg-like cells). Fascicles of tumor cells with spindle morphology were present in all cases, but they represented a minority of the neoplastic population and showed a milder degree of nuclear atypia. All cases showed tumor cells with condensed and deeply eosinophilic cytoplasm and/or nuclei (mummified cells), and focal areas of necrosis that were generally localized in the center of the lesion and associated with leukocytoclasia. Emperipolesis (mainly of neutrophils and eosinophils) was identified in most tumors (6/7 cases, 86%). Mitotic count was generally low, ranging from 1-9 mitoses per 10 high power fields (0.4–3.8 mitoses/mm²). Atypical mitotic figures were seen in a single case (case 1). Most neoplasms were densely cellular, with little intervening stroma, mainly consisting of thick collagen bundles and peripheral areas of fibrosis. In two tumors (28%), the fibrous stroma was more abundant, and the collagen fibers were sometimes arranged surrounding tumor cells. Rare and focal myxoid stromal changes were noted in one case (Fig. 2E), but pseudolipoblasts were absent in all cases. Other findings included abundant high endothelial venules (4 cases, 57%), perineural invasion (2 cases, 28%) and Langhans-type giant cells (1 case, 14%).

Immunohistochemically, the tumor cells focally expressed pan-cytokeratin AE1-AE3 (4/7, 57%) and diffusely expressed Cyclin D1 (4/4, 100%). The following markers were negative: desmin (5/5), S100 (5/5), CD34 (7/7), CD30 (6/6), CD15 (2/2), CD163 (4/4), CD68 (4/4), ALK (2/2), CD3 (1/1), CD20 (1/1), HSV1/2 (2/2), CMV (2/2), and YAP1 (6/6 cases). Of note, the various cellular components of the inflammatory infiltrate were variably positive for several markers (S100, CD15, CD30, CD68, CD163, CD3 and CD20), but the large neoplastic cells were consistently negative. PAS and Ziehl-Neelsen stains performed in 2 cases did not reveal any pathogen.

Cytogenetic findings
Array-comparative genomic hybridization analysis, performed in cases 1, 2, 4 and 7, showed simple genomic profiles lacking significant gene copy number variations (Table 2 and Supple-mentary Fig. 2). In addition, FISH analysis performed in case 3 did not reveal copy number alteration of *VGLL3*.

RNA-Sequencing
RNA-Sequencing analysis revealed *YAP1::MAML2* fusion genes in 3/7 cases (43%, Table 2 and Fig. 3). Two types of fusions were seen; in type one (cases 2 and 5), *YAP1* exon 1 was fused to *MAML2* exon 2; in type 2 (case 7), *YAP1* exon 5 was fused to *MAML2* exon 2, probably due to an intrachromosomal inversion. Case 7 showed an additional fusion transcript involving *TOMM70A* exon 1 and *BRAF* exon 9 (Table 2). All detected fusions were predicted to be in-frame.

Gene expression analysis
Gene expression analysis was performed in 6/7 cases of NN-MIFS and a control group, including classic MIFS (*n* = 8) and SCD34FT/ *PRDM10*-STT (*n* = 15). As illustrated in Fig. 4, unsupervised clustering analysis showed that all NN-MIFS and most classic MIFS formed a common cluster (*n* = 12, cluster 3). The remaining groups included SCD34FT/*PRDM10*-STT (*n* = 15, cluster 1) and a second distinct cluster of classic MIFS (*n* = 2, cluster 2). Altogether,
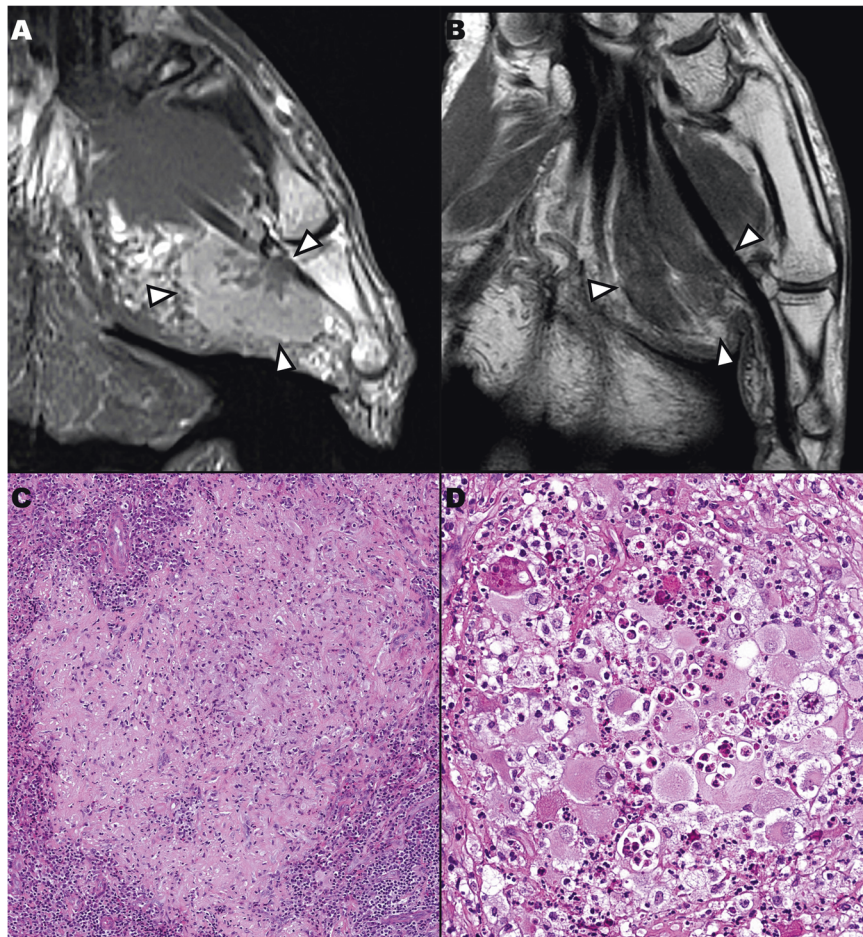
Fig. 1 Radiological and histopathological features of "nodular necrotizing" myxoinflammatory fibroblastic sarcoma (case 5). A Post-contrast T1-weighted MRI performed in 2015, showing a lobulated mass of the right thenar eminence surrounding the tendon of the flexor pollicis brevis muscle (arrows); note the central hypointense "necrotic" areas. **B** Post-contrast T1-weighted MRI performed in 2019, showing complete regression of the mass. **C** Low-power histology of biopsy material, showing a hyalinized tumor lobule surrounded by chronic inflammatory infiltrate. **D** Sheets of epithelioid tumor cells with abundant eosinophilic cytoplasm and large vesicular nuclei with variably prominent nucleoli. Emperipolesis of neutrophils is evident.

these data support that NN-MIFS and MIFS are in the same spectrum.

DISCUSSION

Myxoinflammatory fibroblastic sarcoma is a locally aggressive soft tissue tumor described almost simultaneously in 1998 by three different groups[11–13]. Although its initial characterization was made more than 20 years ago, large comprehensive series of MIFS are scarce, and our understanding of this rare entity remains poor. In this study, we described a peculiar variant of MIFS showing distinctive clinicopathological features associated with a molecular correlate.

Classic cases of MIFS generally form infiltrative masses, which mainly occur in the subcutaneous tissues of acral extremities (hands and feet)[1]. In comparison, NN-MIFS occurred predominantly as well-circumscribed nodules and showed a wider anatomical distribution, with most cases occurring in extra-acral locations (5/7 cases, 71%). Furthermore, the tumors tended to be smaller than the classic MIFS cases described in the two largest series to date (mean size: 20 mm vs. 32 and 42 mm[1,3]) and showed a rather benign clinical course. The latter contrasts with the locally aggressive behavior and high rate of recurrences reported in classic MIFS (~50% of cases). It is also notable that one case of our series showed spontaneous tumor regression. This incompletely

understood phenomenon has been described in an array of neoplasms and it seems to correlate with various molecular alterations (i.e., mutational burden) and tumor-microenvironment interactions[14–16]. Taking into account that MIFS is particularly rich in immune cells, one may suspect that the florid immune response could account for the self-limited case of NN-MIFS and the overall low rate of metastasis of classic MIFS. Apoptosis may also play a role in the biological behavior of NN-MIFS as this was a particularly prominent finding in our series (i.e., mummified cells). It is important to remark that while NN-MIFS showed a good prognosis, the cohort remains small, and future larger studies will be necessary for determining the exact biological potential of these neoplasms. Until a more comprehensive understanding of the disease is achieved, we believe that the management of all variants of MIFS should remain tumor excision with negative margins as this approach has shown to significantly reduce the incidence of local recurrences in classic MIFS[1]. Nonetheless, radical excisions and amputations do not seem reasonable options for the initial management of classic MIFS and NN-MIFS. This type of management should be reserved for locally evolved tumors at presentation or recurring tumors showing aggressive clinical or radiological features. Similarly, while radiotherapy has been proposed to be helpful for the local control of classic MIFS[17], the benefits of its systematic application remains controversial. Altogether, the probable presence of MIFS subsets showing a
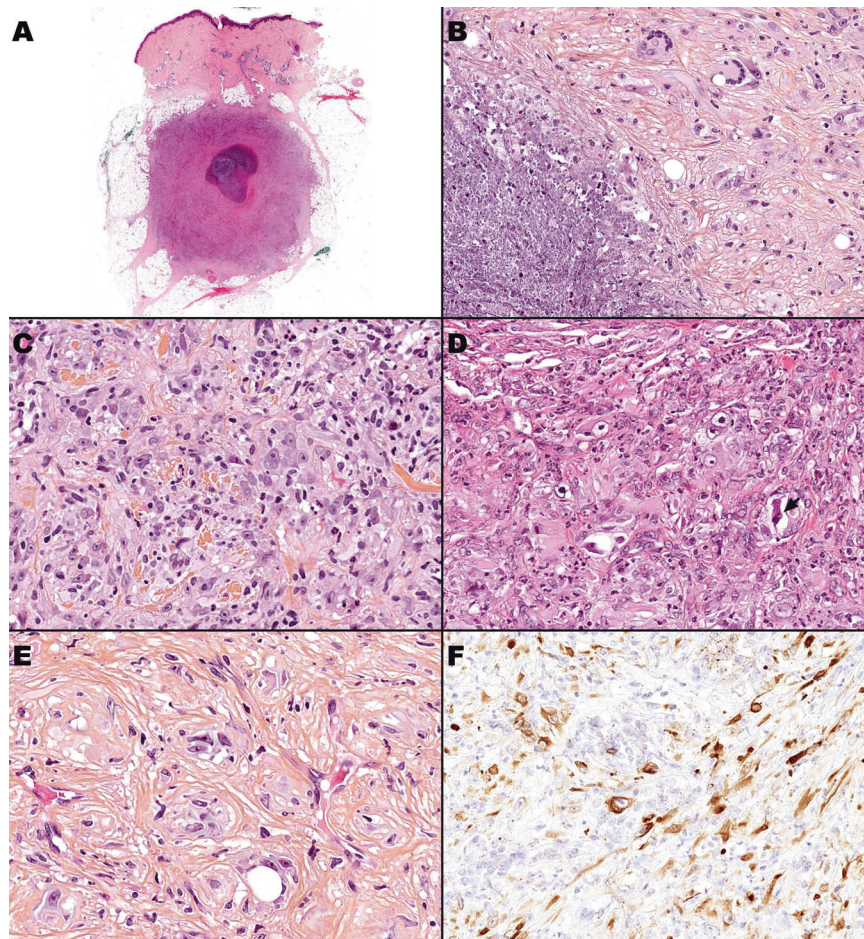
Fig. 2 **Histopathological and immunohistochemical features of "nodular necrotizing" myxoinflammatory fibroblastic sarcoma. A** Case 2, low-power histology showing a relatively well-circumscribed hypodermal nodule with central necrosis. **B** Case 6, high-power view of necrotic areas with leukocytoclasia (left side) and epithelioid tumor cells with Langhans-type multinucleated giant cells (right side). **D**, **E** Case 2 and 6, respectively, sheets of epithelioid tumor cells with abundant eosinophilic cytoplasm and bizarre-looking vesicular nuclei with macronucleoli (virocyte/Reed-Sternberg-like cells), note the abundance of neutrophils and the mummified tumor cell (arrow). **E** Case 6, sclerotic areas composed of thick collagen bundles surrounding nests of tumor cells with very focal myxoid stromal changes (pericellular blueish matrix). The latter was a rare finding seen in an isolated case. **F** Case 2, Pan-keratin (AE1-AE3) expression.

good prognosis stresses the importance of carefully assessing the different treatment strategies used to manage the disease.

From a morphological standpoint, NN-MIFS showed distinctive features: (1) Frequent nodular silhouette, (2) Marked predominance of virocyte/Reed-Sternberg-like cells, (3) Lack or very focal presence of myxoid stromal changes, (4) Presence of central necrotic areas. Many morphological features are shared with classic examples of MIFS, but the latter tends to be larger and more infiltrative or lobulated, has more conspicuous spindle tumor cells and myxoid areas (usually associated with pseudolipoblasts) and rarely shows necrosis. The immunohistochemical analysis of NN-MIFS showed a nonspecific phenotype with focal pan-keratin (AE1-AE3) and Cyclin D1 expression (4/7 and 4/4 cases, respectively). These findings are in agreement with a previous series of classic MIFS except for a slightly more elevated frequency of keratin expression[1]. As remarked by a recent study, specific immunohistochemical markers of MIFS do not currently exist, and its diagnosis remains primarily based on morphological criteria[3]. As MIFS is infrequent and diagnostically challenging, pathologists should be aware of the morphological differential diagnosis, which includes neoplastic and non-neoplastic conditions. An inflammatory or infectious disease could be considered because of the generally dense and polymorphous inflammatory infiltrate, which may include necrosis and giant cells. However, large epithelioid cells with irregular nuclei are not present in inflammatory or infectious conditions. Moreover, both special and immunohistochemical stains for microbes are invariably negative. A pleomorphic sarcoma could also be considered because of the striking atypical cells present in MIFS, which may be abundant, particularly in necrotizing variants. Important clues pointing towards MIFS include a superficial (suprafascial) location, a relatively low mitotic activity (usually < 1 mitosis/mm²), a prominent inflammatory infiltrate, the presence of virocyte or Reed-Sternberg-Like cells and the lack of nuclear hyperchromasia. As portrayed in this study, NN-MIFS consistently shows areas of necrosis, but this feature is generally focal and present in the center of the lesion. In sarcomas, necrosis is typically more abundant and has an irregular distribution. Many morphological features of MIFS overlap with superficial CD34 + Fibroblastic tumor, including superficial location, prominent inflammatory infiltrate, Reed-Sternberg-like cells and focal keratin expression. However, Superficial CD34 + Fibroblastic tumor is diffusely positive with CD34 and rarely shows necrosis[18]. Finally, the presence of Reed-Sternberg-like cells could raise the possibility of Hodgkin-Lymphoma, but exclusive cutaneous presentations of this disease are rare[19], and MIFS is consistently negative with CD30 and CD15.

The widespread application of molecular techniques has allowed a more comprehensive characterization of MIFS. Lambert et al.[20]

Table 2. Molecular features of "nodular necrotizing" myxoinflammatory fibroblastic sarcoma.

Case	Array-CGH and FISH	RNA-Sequencing			
		5' Gene (exon)	5' Gene Breakpoint	3' Gene (exon)	3' Gene Breakpoint
1	Array-CGH: flat profile	—	—	—	—
2	Array-CGH: flat profile	YAP1(1)	101981900	MAML2(2)	95826681
3	FISH: no VGLL3 amplification	—	—	—	—
4	Array-CGH: flat profile	—	—	—	—
5	—	YAP1(1)	101981900	MAML2(2)	95826681
6	—	—	—	—	—
7[a]	Array-CGH: flat profile	YAP1(5)	102076805	MAML2(2)	95826681
		TOMM70A(1)	100119470	BRAF(9)	140487384

Reference Sequence: NM_0011301452 (YAP1); NM_032427 (MAML2); NM_ 004333 (BRAF); NM_014820 (TOMM70A).
[a]Reciprocal products of both chromosomal translocations were detected and highly expressed.

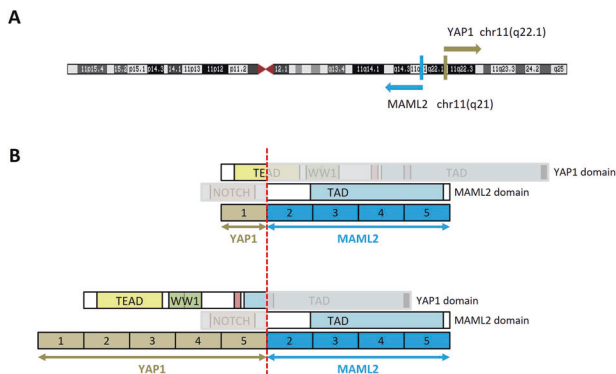**Fig. 3 RNA-Sequencing findings of "nodular necrotizing" myxoinflammatory fibroblastic sarcoma. A** Chromosomal location of YAP1 locus in 11q22.1 and MAML2 in 11q21. Colored lines (blue and brown) depict the genomic breakpoint locus. Arrows indicate the direction of transcription of each gene. **B** Schematic representation of the two types of YAP1::MAML2 fusion transcripts observed in this study. In type 1 fusions, a breakpoint occurs at chr11:101981900(+):: chr11:95826681(-) (hg19), resulting in a YAP1::MAML2 transcript composed of the first exon of YAP1 fused to exons 2 to 5 of MAML2. In type 2 fusions, a breakpoint occurs at chr11:101981900(+):: chr11:95826681(-) (hg19), resulting in a YAP1::MAML2 transcript composed of the first five exons of YAP1 fused to exons 2 to 5 of MAML2. The protein domains of the genes involved in the fusions are also illustrated.

Fig. 4 Gene expression profiling. Unsupervised consensus clustering of a set of 29 tumors performed with all expressed transcripts with an optimal number of clusters of 3 (K = 3). The analysis shows that NN-MIFS and most classic MIFS have similar expression profiles and cluster together (C3). PRDM10-STT and SCD34FT are lumped together in a common cluster (C1), and a small subset of classic MIFS forms a distinct cluster (C2). Clinicopathological and molecular information of the control cohort can be accessed online (Supplementary Table 1). NN-MIFS: nodular necrotizing myxoinflammatory fibroblastic sarcoma, MIFS: myxoinflammatory fibroblastic sarcoma, SCD34FT: superficial CD34 + fibroblastic tumor, PRDM10-STT: PRDM10-rearranged soft tissue tumor.

initially reported a typical case of MIFS in an adult female showing a complex karyotype and a t(1:10)(p22;q24). These findings were corroborated by Hallor et al.[4], and the breakpoints were mapped in (or near) TGFBR3 and OGA (formerly known as MGEA5). The t(1:10) (p22;q24) leads to a non-functional transcript (generally undetectable by RNA-Sequencing) and provokes oncogenic deregulation of various genes, including FGF8 and NPM3. In addition, Hallor et al. demonstrated that MIFS shows a recurrent amplification of VGLL3 (3p12.1). Importantly, none of these anomalies are exclusive to MIFS as TGFBR3 and OGA rearrangements also occur in pleomorphic hyalinizing angiectatic tumor and hemosiderotic fibrolipomatous tumor[6], and VGLL3 amplification in a subset of pleomorphic sarcomas[21]. More recently, Kao et al.[5] showed the presence of BRAF abnormalities in 7 cases of MIFS, including one case with a TOM1L2::BRAF fusion gene. Most cases (4/7, 57%) showed a concomitant amplification of VGLL3, but all 7 cases lacked OGA and TGFBR3 rearrangements. Interestingly, a subset of the cases reported by Kao et al. and the cases from our study showed similar morphological features (i.e., predominantly solid growth with abundant plump epithelioid cells and very focal
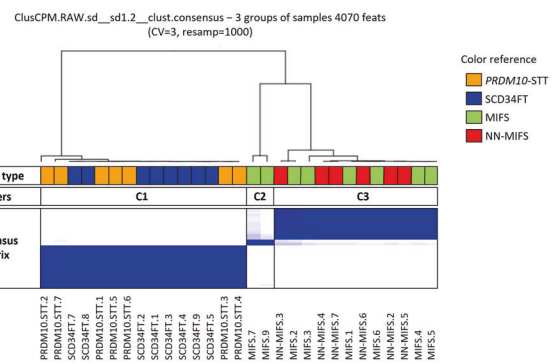
myxoid change). As one of the cases from our series presented a BRAF rearrangement, we wonder whether a potential link between NN-MIFS and BRAF rearranged MIFS may exist. Of note, the single case with BRAF genetic abnormalities seen in our study (case 7) showed a fusion of exon 1 of TOMM70A to exon 9 of BRAF and a concomitant YAP1::MAML2 fusion. As in the index case of Kao et al., the putative chimeric protein from the BRAF fusion is predicted to be oncogenic as it retains the kinase domain of BRAF (C-terminal) and loses its autoinhibitory domains (N-terminal).

While the molecular anomalies reported in MIFS are abundant, their incidence remains somewhat controversial. In the most extensive series of molecularly characterized MIFS, VGLL3 amplification was detected in 8 out of 20 cases (40%), BRAF abnormalities in 4 out of 70 cases (5%), and OGA and TGFBR3 rearrangements in 3 out of 54 cases (5%)[3]. The detection of recurrent YAP1::MAML2 fusions in our study further enriches the complex molecular landscape of MIFS. This translocation seems to occur through a chromosomal inversion which results in the fusion of exon 5 or exon 1 of YAP1 to exons 2 to 5 of MAML2. YAP1::MAML2 translocations have been reported in poroid neoplasms[22], metaplastic thymoma[23], composite and retiform hemangioendothelioma[24], and more recently in spindle cell/ sclerosing rhabdomyosarcoma[25]. YAP1 (Yes1 Associated

Transcriptional Regulator) is a crucial effector of the Hippo signaling pathway, which regulates cell growth and apoptosis. *YAP1* is a transcriptional co-activator that binds to the TEAD family of transcriptional factors to regulate gene transcription. In keeping with previous findings, both types of fusions detected in NN-MIFS are predicted to produce a chimeric protein that retains the N-terminal *YAP1* TEAD binding domain and loses the TAD domain, which is necessary for proteasomal degradation[26]. These alterations ultimately lead to oncogenesis through deregulated TEAD-dependent *YAP1* activity. The function of the C-terminal partner MAML2 is not entirely understood but as the transactivation domain is retained, it may also play a role in the oncogenic activity of the chimeric protein. Notably, both fusion-positive and negative cases of NN-MIFS seem to lack *VGLL3* amplification.

In conclusion, we have described a variant of MIFS commonly occurring in extra-acral sites and characterized by a frequent nodular configuration, predominance of atypical epithelioid cells (Reed-Sternberg-like cells), scant or absent myxoid stromal changes and consistent presence of necrosis. These NN-MIFS variants frequently show focal pan-keratin (AE1-AE3) expression and *YAP1::MAML2* fusions. In contrast to classic MIFS, NN-MIFS seems to show a rather benign clinical course, which warrants future confirmation in a more extensive series.

DATA AVAILABILITY
The datasets used and/or analyzed during the current study are available from the corresponding author on reasonable request.

REFERENCES

1. Laskin, W. B., Fetsch, J. F. & Miettinen, M. Myxoinflammatory fibroblastic sarcoma: A clinicopathologic analysis of 104 cases, with emphasis on predictors of outcome. *Am J Surg Pathol* **38**, 1–12 (2014).
2. WHO Classification of Tumours Editorial Board. WHO Classification of Tumours of Soft Tissue and Bone, 5th ed. Lyon, France: IARC Press (2020).
3. Suster, D., Michal, M. & Huang, H. et al. Myxoinflammatory fibroblastic sarcoma: an immunohistochemical and molecular genetic study of 73 cases. *Mod Pathol* **33**, 2520–2533 (2020).
4. Hallor, K. H., Sciot, R. & Staaf, J. et al. Two genetic pathways, t(1;10) and amplification of 3p11-12, in myxoinflammatory fibroblastic sarcoma, haemosiderotic fibrolipomatous tumour, and morphologically similar lesions. *J Pathol* **217**, 716–727 (2009).
5. Kao, Y. C., Ranucci, V. & Zhang, L. et al. Recurrent BRAF Gene Rearrangements in Myxoinflammatory Fibroblastic Sarcomas, but Not Hemosiderotic Fibrolipomatous Tumors. *Am J Surg Pathol* **41**, 1456–1465 (2017).
6. Antonescu, C. R., Zhang, L. & Nielsen, G. P. et al. Consistent t(1;10) with rearrangements of TGFBR3 and MGEA5 in both myxoinflammatory fibroblastic sarcoma and hemosiderotic fibrolipomatous tumor. *Genes Chromosomes Cancer* **50**, 757–764 (2011).
7. Anders, S., Pyl, P. T. & Huber, W. HTSeq-a Python framework to work with high-throughput sequencing data. *Bioinformatics* **31**, 166–169 (2015).
8. Team DC. R: A Language and Environment for Statistical Computing (2017).
9. Wilkerson, M. D. & Hayes, D. N. ConsensusClusterPlus: A class discovery tool with confidence assessments and item tracking. *Bioinformatics* **26**, 1572–1573 (2010).
10. Law, C. W., Chen, Y. & Shi, W. et al. voom: Precision weights unlock linear model analysis tools for RNA-seq read counts. *Genome Biol* **15**, R29 (2014).
11. Meis-Kindblom, J. M. & Kindblom, L. G. Acral myxoinflammatory fibroblastic sarcoma: a low-grade tumor of the hands and feet. *Am J Surg Pathol* **22**, 911–924 (1998).
12. Montgomery, E. A., Devaney, K. O. & Giordano, T. J. et al. Inflammatory myxohyaline tumor of distal extremities with virocyte or Reed-Sternberg-like cells: a distinctive lesion with features simulating inflammatory conditions, Hodgkin's disease, and various sarcomas. *Mod Pathol* **11**, 384–391 (1998).
13. Michal, M. Inflammatory myxoid tumor of the soft parts with bizarre giant cells. *Pathol Res Pr* **194**, 529–533 (1998).
14. Franses, J. W., Bhan, I. & Pankaj, A. et al. Spontaneous Immune-Mediated Regression of Hepatocellular Carcinoma With High Tumor Mutational Burden. JCO Precis. *Oncol* **17**, 5 (2021).
15. Sápi, Z., Lippai, Z. & Papp, G. et al. Nodular fasciitis: a comprehensive, time-correlated investigation of 17 cases. *Mod Pathol* **34**, 2192–2199 (2021).
16. Marquina, G., Sanchez-Ramon, S. & Sarnago, A. et al. Complete Spontaneous Regression of Lung Metastases after Resection of CIC-Rearranged Sarcoma: A Case Report. *Case Rep. Oncol* **14**, 152–159 (2021).
17. Tejwani, A., Kobayashi, W. & Chen, Y.-L. E. et al. Management of acral myxoinflammatory fibroblastic sarcoma. *Cancer* **116**, 5733–5739 (2010).
18. Perret, R., Michal, M. & Carr, R. A. et al. Superficial CD34-positive fibroblastic tumor and PRDM10-rearranged soft tissue tumor are overlapping entities: a comprehensive study of 20 cases. *Histopathology* **79**, 810–825 (2021).
19. Huong, G., Olson, L. C. & Rippis, G. E. et al. An Index Case of Cutaneous Hodgkin Lymphoma and Review of the Literature. *Am J Dermatopathol* **38**, 739–743 (2016).
20. Lambert, I., Debiec-Rychter, M. & Guelinckx, P. et al. Acral myxoinflammatory fibroblastic sarcoma with unique clonal chromosomal changes. *Virchows Arch* **438**, 509–512 (2001).
21. Hélias-Rodzewicz, Z., Pérot, G. & Chibon, F. et al. YAP1 and VGLL3, encoding two cofactors of TEAD transcription factors, are amplified and overexpressed in a subset of soft tissue sarcomas. *Genes Chromosomes Cancer* **49**, 1161–1171 (2010).
22. Sekine, S., Kiyono, T. & Ryo, E. et al. Recurrent YAP1-MAML2 and YAP1-NUTM1 fusions in poroma and porocarcinoma. *J Clin Invest* **129**, 3827–3832 (2019).
23. Vivero, M., Daviveni, P. & Nardi, V. et al. Metaplastic thymoma: a distinctive thymic neoplasm characterized by YAP1-MAML2 gene fusions. *Mod Pathol* **33**, 560–565 (2020).
24. Antonescu, C. R., Dickson, B. C. & Sung, Y.-S. et al. Recurrent YAP1 and MAML2 Gene Rearrangements in Retiform and Composite Hemangioendothelioma. *Am J Surg Pathol* **44**, 1677–1684 (2020).
25. Cordier, F., Ameloot, E. & Dhooge, C. et al. Spindle cell/sclerosing rhabdomyosarcoma with a novel YAP1-MAML2 fusion in a 1-year-old: not all strongly TRK-expressing spindle cell sarcomas in infants are infantile fibrosarcomas! *Pathology* **53**, 936–939 (2021).
26. Szulzewsky, F., Holland, E. C. & Vasioukhin, V. YAP1 and its fusion proteins in cancer initiation, progression and therapeutic resistance. *Dev Biol* **475**, 205–221 (2021).

AUTHOR CONTRIBUTIONS
RP performed the study concept, design, data acquisition and writing of the paper; MT, GDP, JMC and FLL participated in the study concept and provided data; GB provided clinical data; VV performed immunohistochemical assays and provided technical assistance; IS participated in the interpretation of genomic assays (aCGH and FISH); JB and RA performed RNA-Sequencing based techniques, contributed to the interpretation of data and performed bioinformatics analysis. JB designed Fig. 3. All authors read and approved the final paper.

COMPETING INTERESTS
The authors declare no competing interests.

ETHICS APPROVAL AND CONSENT TO PARTICIPATE
This study was conducted following local ethical guidelines. All cases are recorded in the national sarcoma pathology RREPS database, approved by the National Committee for Protection of Personal Data (CNIL, no. 910390) in alignment with the ethical principles of the Helsinki Declaration.

ADDITIONAL INFORMATION
Supplementary information The online version contains supplementary material available at https://doi.org/10.1038/s41379-022-01096-6.

Correspondence and requests for materials should be addressed to Raul Perret.

Reprints and permission information is available at http://www.nature.com/reprints

Publisher's note Springer Nature remains neutral with regard to jurisdictional claims in published maps and institutional affiliations.